Extreme Mechanics Letters 40 (2020) 100980

Contents lists available at ScienceDirect

Extreme Mechanics Letters

journal homepage: www.elsevier.com/locate/eml

Hard auxetic metamaterials

Finn Box [a,*], Chris G. Johnson [b], Draga Pihler-Puzović [a]

[a] Department of Physics & Astronomy and Manchester Centre for Nonlinear Dynamics, University of Manchester, Oxford Road, M13 9PL, Manchester, UK

[b] Department of Mathematics and Manchester Centre for Nonlinear Dynamics, University of Manchester, Oxford Road, M13 9PL, Manchester, UK

ARTICLE INFO

Article history:
Received 27 July 2020
Received in revised form 8 September 2020
Accepted 13 September 2020
Available online 15 September 2020

Keywords:
Mechanical metamaterials
Auxetics
Poisson's ratio
Buckling instabilities
Metals
Plastics

ABSTRACT

Auxetics are materials that contract laterally when compressed, rather than expand, in contrast to common experience. Here we show that common metals and plastics can be rendered auxetic through the introduction of a regular array of holes. Under compression, these hard holey materials bypass localized failure modes, such as shear banding, and instead deform via a global pattern transformation previously reported in elastomeric structures. Despite significant variations in internal structure, the pattern transformation responsible for auxetic behaviour in both metals and plastics is governed by the buckling of the slender struts that comprise the microarchitecture. Furthermore, in contrast to elastomeric structures, holey sheets made from hard materials exhibit significant negative post-buckling stiffness. This suggests that, beyond the geometrical nonlinearities associated with topological modifications, material nonlinearities which arise during plastic deformation offer further potential for altering the material properties of the constituent.

1. Introduction

The Poisson's ratio ν is a measure of the transverse-to-axial strain in a loaded material. Auxetic materials, for which $\nu < 0$, exhibit counter-intuitive lateral contraction when compressed uni-axially [1–9] and are valued for their desirable material properties, e.g. enhanced hardness and vibration absorption (relative to their non-auxetic counterparts [4]). Auxetic behaviour can be engineered into soft materials by harnessing elastic buckling instabilities [10–17], resulting in flexible mechanical metamaterials. Typically made from an elastomer for which $\nu \simeq 0.5$, the auxetic response arises as a consequence of small-scale topological changes to the bulk (namely, the introduction of voids) that introduce a microarchitecture [18] into the material. Indeed, the archetypal auxetic metamaterial is an elastic sheet perforated with a dense square array of regular holes [10–13,16]. Under compression, elastic buckling of the interhole ligaments causes the circular holes to transform into mutually orthogonal ellipses, resulting in a lateral contraction of the sheet. These soft, holey sheets have found application in phononics [19,20] and photonics [21,22], as wave guides [23] and in colour displays [24]. Industrial application is limited, however, by the material properties of the bulk, in particular; the low strength, low melting point and low resistance to chemical corrosion of the base elastomer.

Metals, in particular, serve as attractive base materials for strong, durable metamaterials. However, at the bulk scale, metals contain many defects such as dislocations, grains and microcracks that could induce the early onset of plasticity and inhibit buckling in periodic, porous structures [25]. (Even a solid column under axial compression, which has a fully stable post-buckling behaviour in the elastic range, is appreciably affected by small imperfections in the plastic range [26].) As such, the use of metals and metallic alloys in the creation of mechanical metamaterials with auxetic properties remains relatively unexplored. Pattern transformation and auxetic behaviour have been reported in atomistic simulations of holey metallic nanostructures [25] when the plate thickness approaches the nanoscale, due to a free surface effect that induces a finite compressive stress inside the nanoplates [27]. Experimentally, an auxetic response has been observed under compression in a cellular metal that was fabricated with a partial imprint of the desired deformation pattern [28], and under tension in metal sheets sparsely patterned with mutually orthogonal elliptical slots [29]. However, neither of these cases exhibit a symmetry-breaking pattern transformation (as discussed in [30]) since the pattern of deformation simply reflects the structure prescribed by the undeformed sample. Specifically, the Poisson's ratio of the bulk material is recovered [29], or shear banding occurs [28], as the aspect ratio of the holes approaches 1 (circular holes).

Here, we demonstrate symmetry-breaking pattern transformation and auxetic behaviour in holey sheets of crystalline metals and semi-crystalline thermoplastics, as shown in Fig. 1. Although pattern transformation requires plastic deformation, which depends on the internal structure of the material, the phenomenon

* Corresponding author.
E-mail address: finn.box@manchester.ac.uk (F. Box).

https://doi.org/10.1016/j.eml.2020.100980

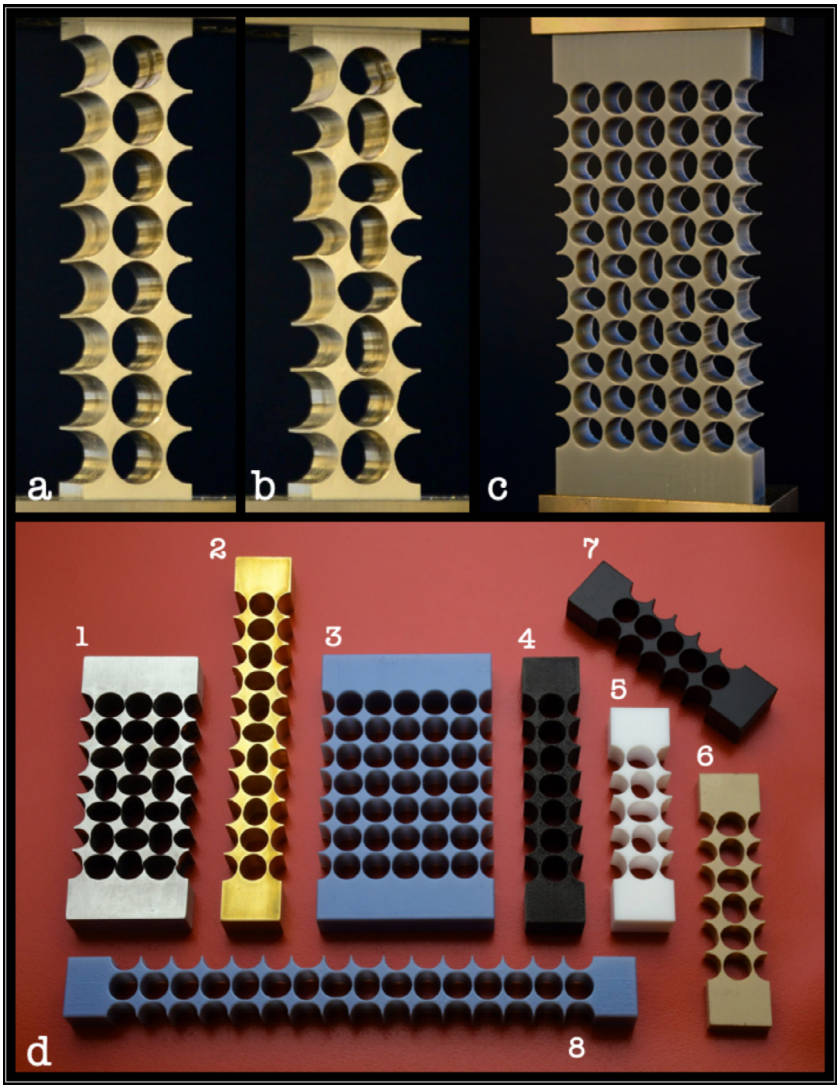

Fig. 1. Pattern switching in metals and plastics. a–b. Uniaxial compression of a holey column (machined from aluminium plate and annealed) triggers a pattern transformation whereby neighbouring holes become orthogonal ellipses. c. A holey sheet (made from polylactic acid (PLA) using a 3D printer) also exhibits pattern transformation following compression. d. Strain-induced pattern transformation in samples fabricated from: 1. Aluminium, 2. Brass, 3. 3D-printed plastic (PLA), 4. Reinforced 3D plastic, 5. Polytetrafluoroethylene (PTFE), 6. Polyether ether ketone (PEEK), 7. Nylon, and 8. PLA.

is instead governed by an elastic buckling instability; the unbuckled solution bifurcates for a critical stress that depends on the compressive stiffness of the struts that comprise the microarchitecture. Material nonlinearities do play a role, however, as these hard holey structures exhibit significantly different post-buckling behaviour to their elastic counterparts.

2. Experiments

Our experimental samples were fabricated from a variety of hard materials using standard manufacturing techniques (see Appendix A for details). The bulk Young's modulus of the materials used was measured and found to be in the range $0.49 \leq E_{bulk} \leq 11.1\,\mathrm{GPa}$. All samples had a hole diameter $D = 8\,\mathrm{mm}$ and minimum strut thickness $t = 0.5\,\mathrm{mm}$, so that the hole centres were $L_0 = 8.5\,\mathrm{mm}$ apart, and $t/L_0 < 0.06$. The width and height of the samples depended on the number of holes in the array; tests were performed on columns, $N_C = 1$, with $5 \leq N_R \leq 21$ rows, and sheets of $5 \leq N_R \leq 11$ rows with $2 \leq N_C \leq 5$ columns. Samples were typically of depth $d = 12.7\,\mathrm{mm}$, although samples of depths $d = 6.5$, 6.6 and 10.1 mm were also tested. At each end of the sample, a length of solid material, $l_{ends} = 12\,\mathrm{mm}$, was left free from holes. The ends were placed inside custom-built adaptors that prevented horizontal displacement of the sample during testing and subsequent formation of localized shear bands (discussed elsewhere [28,31]).

Compressive testing was performed using a Universal Testing System (5569, Instron). Stress–strain curves were calculated from the acquired force–displacement data: specifically, the engineering stress $\sigma = F/A$ is the ratio of the compressive force F to the top surface area $A = (N_C + 1)L_0 d$, which depends on the number of columns in the array; and the engineering strain $\epsilon = \Delta l/l_0$ is the ratio of the change in sample length, Δl, to the initial sample length, $l_0 = N_R L_0 + 2l_{ends} - t$, which includes the solid material at each end of the structure.

A dependence of the pattern transformation on strain rate has been reported in plastic cellular structures [31]. We believe, however, that the shear banding reported therein for low rates of compression was a consequence of samples being free to slide horizontally over the testing platform, rather than being held in place during compression (as in the case here). We instead observe a global pattern transformation in holey structures made from a variety of polymer-based plastics and for a wide range

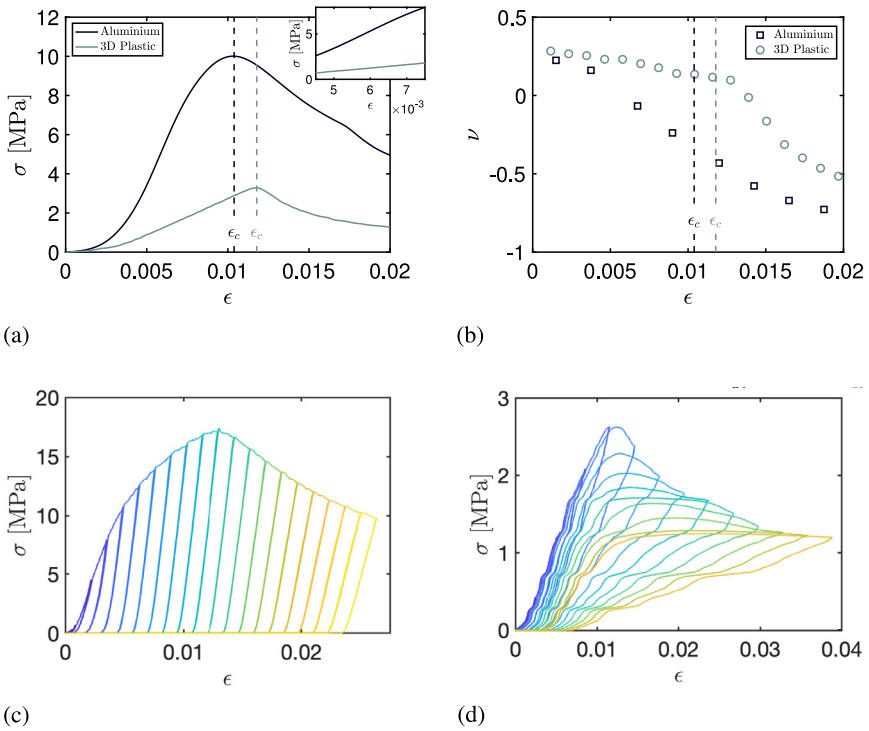

Fig. 2. Stress–strain and auxetic response of hard, holey materials. a. Stress–strain response of holey sheets machined from aluminium and 3D-printed in plastic; the experimental samples comprised a 3 × 7 and a 5 × 7 array of circular holes, respectively. Inset: the approximately linear response prior to pattern switching. b. Poisson's ratio ν as a function of applied axial strain, computed from the measured centre-to-centre displacement of the 9 central holes in each sample from (a); in both samples, ν changes from positive to negative as the axial strain increases. In a–b: vertical dashed lines indicate the critical engineering strain, ϵ_c, for which the maximum applied stress is recorded. c–d. Mechanical response to incremental, cyclic loading of: (c) an aluminium column with a 1 × 6 array of circular holes, which yields (deforms plastically) for small strains $\epsilon \ll \epsilon_c$, and (d) a plastic (nylon) column with a 1 × 5 array of circular holes, which deforms elastically until the strain exceeds the critical value for pattern switching; plastic deformation only occurs for $\epsilon \gtrsim \epsilon_c$. (Cycling loading of other samples, e.g. plastic samples with a 1 × 6 array of circular holes, yields qualitatively similar results). In c–d: different load cycles are represented by different colour curves ranging from low strain (blue) to high strain (yellow). (For interpretation of the references to colour in this figure legend, the reader is referred to the web version of this article.)

of strain rates. In particular, a symmetry-breaking buckling instability occurred in holey columns compressed at rates in the range 0.001–8.5 mm s^{-1} (metals and plastics), and in holey sheets compressed at rates in the range 0.001–1 mm s^{-1} (plastics) and 1–8.5 mm s^{-1} (metals). The deformation of holey samples was imaged using a Nikon D7100 camera and measured via image processing techniques developed in MATLAB.

3. Results

Fig. 1a shows a holey column fabricated from aluminium. Uniaxial compression of the sample triggers a pattern switch whereby the array of initially circular holes is transformed into an array of mutually orthogonal ellipses, shown in Fig. 1b. The observed pattern transformation is strikingly similar to that previously reported in soft cellular solids [10–17,31–33]. Samples of various size, fabricated from different materials, are shown in Fig. 1c–d following compression, clearly demonstrating that strain-induced pattern switching also occurs in both metallic and plastic materials.

Stress–strain curves for holey sheets made from aluminium and plastic are shown in Fig. 2a. Both samples exhibit similar stress–strain curves, including a linear region for relatively small strains, wherein stress is approximately proportional to applied strain (see inset to Fig. 2a), and a pronounced peak beyond which decreasing stiffness is observed for increasing deformation. Strain-softening is not observed in the bulk materials used for producing the samples; instead, they strain harden beyond the yield point. Negative post-buckling stiffness has been reported in wide elastic metabeams [34], honeycombs [35,36] and elastic porous structures containing a small number of holes [32,37]. However, under compression (and without lateral confinement [14,17]), elastic sheets containing a square array of $\gtrsim$ 10 circular holes instead exhibit a stress-plateau [10–13] which suggests that the pronounced strain-softening observed here is a consequence of material nonlinearities that emerge during irreversible, plastic deformation.

Notably, even though the number of holes in the samples is different, and the Young's modulus of the bulk material differs by a factor 5, the critical strain at peak stress, $\epsilon_c = \epsilon(\sigma_c)$, is comparable between the two samples. Later, we demonstrate that this is a consequence of the two samples having identical microarchitecture. First, we turn our attention to the negative Poisson's ratio behaviour exhibited by the samples.

Following the procedure outlined in [12] we compute the Poisson's ratio ν of the samples during compression by measuring the centre-to-centre displacement of the holes, in the horizontal and vertical directions. The results are shown in Fig. 2b and clearly demonstrate that ν changes from positive to negative with increasing strain. This implies that, for small compressive strains, the samples expand laterally; whereas, for large strains, the samples instead contract. These measurements also highlight a marked difference in the mechanical response of metal and plastic samples to increasing strain. In a manner similar to that exhibited in elastic cellular solids [12], the measured Poisson's ratio of the plastic sample remains positive, and approximately constant, until the strain reaches ϵ_c and then switches to negative for $\epsilon > \epsilon_c$. The aluminium sample, however, shows an approximately linear decrease in the Poisson's ratio with increasing strain and, as such, becomes negative for $\epsilon < \epsilon_c$.

To better understand the different auxetic response of metals and plastics, we performed incremental cyclic loading tests;

samples were repeatedly compressed, with increasing applied strain. The results, shown in Figs. 2c–d, evidence clear distinctions between metal and plastic samples. Aluminium samples deform plastically for strains far below the critical strain for pattern transformation (Fig. 2c) which suggests that compression is accommodated through plastic deformation before pattern switching occurs, and that yield is therefore responsible for the early onset of negative ν measured for $\epsilon < \epsilon_c$. In contrast, the deformation of plastic samples is reversible (to some degree) for strains $\epsilon > \epsilon_c$ and yield only occurs once the strain becomes comparable to the critical strain for pattern transformation (Fig. 2d), $\epsilon \approx \epsilon_c$; beyond this point, significant hysteresis is observed.

Having shown that plastic deformation permits a novel route to a negative Poisson's ratio, we now explore the role of the microarchitecture in the pattern transformation responsible for auxetic behaviour. In elastic cellular solids, buckling of the ligaments that surround the holes induces rotation of the joints that connect the ligaments [10,12]. To find out if this is also the case in cellular solids made from hard materials, we tested the mechanical response of a single strut – the simplest structural element of the microarchitecture – to the three modes of deformation: compression, shear and rotation. Schematic diagrams of the structural elements, and the testing procedures used, are shown in Fig. 3a. The dimensions of the structural elements were identical to those found in the microarchitecture of our experimental samples, and tests were performed on the same structural testing system.

Force–displacement curves for the structural elements comprising the microarchitecture are shown in Fig. 3b. Evidently the thin geometry of the struts means that the compressive stiffness of a single strut is much greater than either its shear or bending stiffness. We define an effective elastic moduli of a single strut $E_{strut} = (F/A_s)/(\Delta l_s/l_s)$, where $A_s = w_s d$ is the area of the base of the strut ($w_s = 8.5$ mm and $d = 12.7$ mm), $l_s = 12.7$ mm is its initial vertical length and Δl_s is the change in that length (see Fig. 3a). This provides a measure of the strut's ability to withstand changes in length when subject to compressive forces. For 3D struts printed in plastic, we measured $E_{strut} = 0.15 \pm 0.01$ G Pa; while for brass struts, $E_{strut} = 1.79 \pm 0.4$ G Pa. (The annealing of dimensionally-accurate aluminium struts proved a technical challenge and, as such, they were not tested). The measured values of the effective compressive stiffness of a single strut were significantly smaller than the Young's modulus of the bulk material, $E_{bulk}/E_{strut} \sim \mathcal{O}(10)$. Using these measurements we now demonstrate that the global pattern transformation responsible for auxetic behaviour in hard materials is indeed governed by the mechanical properties of the microarchitecture.

In Figs. 3c–d, we show the measured critical strain, $\epsilon_c = \epsilon(\sigma_c)$, for holey columns and holey sheets made from various materials and of different sizes (coloured, filled markers) as a function of the number of struts in the sample, $N_{struts} = N_C(N_R-1)+N_R(N_C+1)$. Recalling that for small strains, stress is approximately proportional to applied strain $\sigma = E_{bulk}\epsilon$, where E_{bulk} is the Young's modulus of the bulk material, we include the measured value of the dimensionless peak stress σ_c/E_{bulk} in Figs. 3c–d (coloured, empty markers). An order of magnitude discrepancy exists between measured values of ϵ_c and σ_c/E_{bulk}. However, ϵ_c is in better agreement with σ_c/E_{strut} (also plotted on the figure; black markers) which suggests that the mechanical response of the samples is dominated by the pre-buckling compressive stiffness of the microarchitecture, rather than the compressive stiffness of the bulk material. This is consistent with theoretical modelling [33], which indicates that compression of the inter-hole ligaments, a property of the microstructure, controls the overall pre-buckling stiffness of a perforated structure. Consequently, (*i*) a rigid sheet of solid matter can be softened considerably by introducing a periodic, porous microarchitecture, and (*ii*) the global pattern transformation responsible for the auxetic response is instigated by the buckling of the struts that comprise the microarchitecture.

4. Modelling

We now compare our results on hard, holey structures to a model of the aforementioned elastic, cellular solids to see if the critical buckling stress of metal and plastic structures can be predicted from the elastic behaviour of their individual structural elements (or 'building blocks'). When the minimum thickness of material between holes in a Neo-Hookean elastic cellular structure is small compared to the hole diameter, $t/L_0 \ll 1$, the bending occurs predominantly in these thin struts. This allows simple asymptotic modelling to predict the critical buckling stress of long columns [33]. Buckling of a structure with $N_R \geq 2$ rows by $N_C \geq 1$ columns of holes involves bending of $(N_R-1)N_C + (N_C+1)N_R$ struts. Each strut is assumed to bend at its thinnest point, and, for small deformations, exert a bending moment $M = \kappa\theta$ that is linear in the bending angle θ, where κ is the bending stiffness of the strut. This bending moment was measured experimentally for a single, plastic strut in the experimental configuration illustrated in Fig. 3a(iii). In this experiment, a force was applied at a perpendicular distance $x = L_0/2 = 4.25$mm from the strut, and the measured stiffness was found to be $F/\Delta l = 1.3 \times 10^4$ N m^{-1}. From the definition of a moment $M = \kappa\theta = FL_0/2$ and the geometric relationship between the angle of bending and the displacement at the point of applied force $\theta = \Delta l/x$ we find

$$\kappa = \frac{FL_0^2}{4\Delta l} = 0.234\,\text{N m}. \tag{1}$$

When the structure is compressed with a force F and each strut is bent by an angle θ, the height of the solid is reduced by $N_R L_0(1-\cos(\theta/2))$. Extending the argument of [33] to structures with more than one column results in a potential energy

$$V = \frac{1}{2}\left[(N_R-1)N_C + (N_C+1)N_R\right]\kappa\theta^2 + N_R L_0\left[\cos\left(\frac{\theta}{2}\right)-1\right]F. \tag{2}$$

The equilibria lie at the stationary points of this energy, i.e. for $\partial V/\partial\theta = 0$ where

$$\frac{\partial V}{\partial\theta} = \left[(N_R-1)N_C + (N_C+1)N_R\right]\kappa\theta - \frac{N_R L_0}{2}\sin\left(\frac{\theta}{2}\right)F, \tag{3}$$

and the bifurcation in the unbuckled equilibrium solution, $\theta = 0$, lies at a critical force

$$F_c = 4\left[1 + N_C\left(2 - \frac{1}{N_R}\right)\right]\frac{\kappa}{L_0}. \tag{4}$$

Dividing this by the area of the top of the structure, $(N_C+1)L_0 d$, gives the critical stress

$$\sigma_c = 4\left(1 + \frac{N_C(N_R-1)}{N_R(N_C+1)}\right)\frac{\kappa}{L_0^2 d}, \tag{5}$$

which can be nondimensionalized with respect to the Young's modulus of the bulk E_{bulk} or a strut E_{strut}, as is shown by the dot-dashed and dashed lines in Figs. 3c–d, respectively. (Note that in Fig. 3c this asymptotic prediction is shown in the limit of a tall column, i.e. for $N_C = 1$ and $N_R \gg 1$.) The reasonable agreement between predictions of the elastic buckling stress and measurements in hard materials is remarkable considering the intrinsic differences in material properties, and the manifestation of material nonlinearities during plastic deformation. However, we acknowledge that, from the definition of E_{strut}, the quantity σ_c/E_{strut} is simply the engineering strain ϵ of the structure that would be observed if each strut behaved identically to the

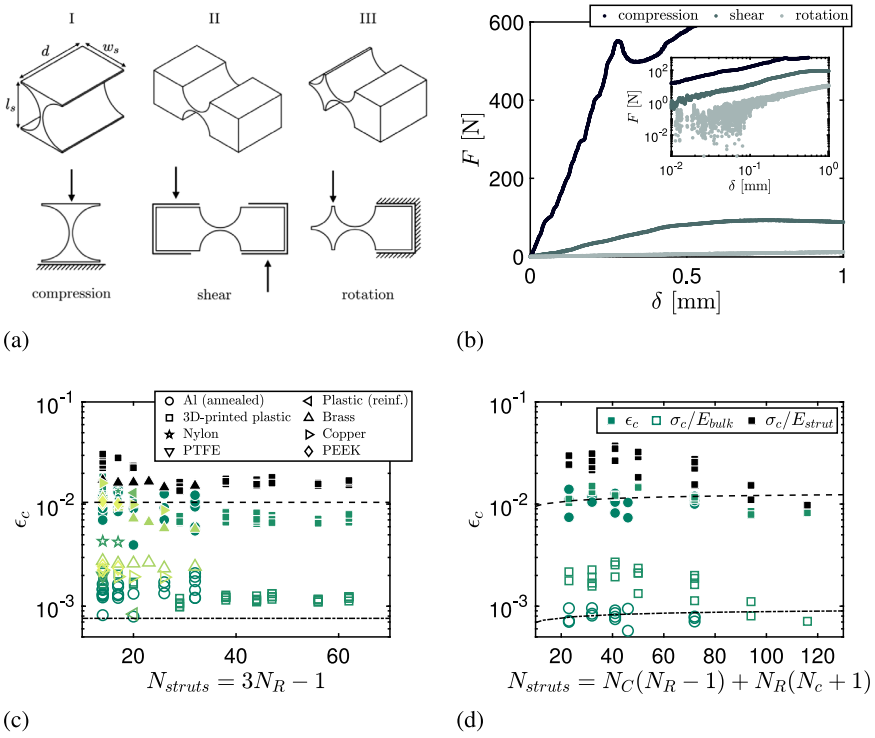

Fig. 3. Strut stiffness controls the critical strain. a. Schematic diagrams of the elements used to test the mechanical response of a structural element to three modes of deformation (compression, shear and rotation). b. Force–displacement curves for elements subject to axial compression, shear and rotation. Inset: raw data on a log–log plot. The compressive stiffness of a single strut is orders of magnitude larger than the shear or rotational stiffnesses. An effective modulus of compressive stiffness of a single strut is given by $E_{strut} = (F/A_s)/(\delta/l_s)$, where $A_s = w_s d$ is the area of the base/top of the strut, l_s is its initial vertical length and δ is the vertical displacement of the testing system, which exactly corresponds to the change in length of the sample Δl_s during compressive deformation. c–d. Critical strain as a function of the number of struts in: (c) holey columns, $N_C = 1$ and $5 \leq N_R \leq 21$, made from different materials (as indicated in the legend), and (d) holey sheets machined from aluminium or printed from plastic ($2 \leq N_C \leq 5$ and $5 \leq N_R \leq 11$). In c–d: filled, coloured markers represent the measured critical strain ϵ_c; empty, coloured markers represent σ_c/E_{bulk}; and black markers represent σ_c/E_{strut} (as indicated in the legend to Fig. 3.d). Also shown are asymptotic predictions of σ_c/E_{bulk} (dot-dashed line) and σ_c/E_{strut} (dashed line), as given by Eq. (5), for (c) the limit of tall, holey columns (for which $N_C = 1$ and $N_R \gg 1$) and (d) sheets with $N_R \geq 2$ rows and $N_C \geq 2$ columns of holes. (For interpretation of the references to colour in this figure legend, the reader is referred to the web version of this article.)

isolated compressed strut (Fig. 3a(i)). The observed engineering strain at bifurcation ϵ_c is a factor of $\sim$2 smaller than this for structures with $N_{struts} \lesssim 100$, suggesting that the effects of microplasticity [38] may be non-negligible in structures comprising a small number of holes.

5. Discussion

Metallic metamaterials with multiscale, hierarchical microarchitectures have been reported previously [39]. However, the fabrication of these fractal-like materials requires complex, additive manufacturing techniques. Here we have demonstrated that auxetic metamaterials can be fabricated from hard materials merely by perforating metal or plastic sheets with a regular array of holes, so could be readily incorporated into industrial manufacturing processes (or realized by a home enthusiast with a suitable drill). The resultant structures are: low density, being comprised mainly of voids; high strength, relative to their elastic counterparts; can withstand high temperatures; and are resistant to chemical wear and corrosion. The remarkable agreement between the measured critical stress at which hard metamaterials undergo pattern-switching and the critical buckling stress predicted using our model for elastic cellular solids suggests that the behaviour of hard structures is dominated by elastic deformations of the structural elements comprising the microarchitecture (at least prior to the global pattern switch). Similarly, elastic properties of microarchitecture determine failure process in brittle rocks [40], for example.

Above a critical load, these holey structures deform plastically, absorbing mechanical energy in the process [41]. As such, they provide a novel solution for the practical fabrication of low-weight, crumple zones – for use in trains and automobiles – and other impact-absorbing structures [42,43]. Furthermore, these engineered structures fold-in on themselves during compression (rather than expanding, or failing via the formation of collapse bands [44–47]). This implies that failure modes which typically arise during plastic deformation, such as strain localization, can be bypassed by harnessing elastic buckling of the structural elements present in the microarchitecture. Material nonlinearities which emerge during plastic deformation can results in further, surprising changes to the mechanical properties of the bulk material, such as negative stiffness. Harnessing material nonlinearities could therefore provide further tools for designing the macroscale, mechanical behaviour of metamaterials made from hard materials.

Declaration of competing interest

The authors declare that they have no known competing financial interests or personal relationships that could have appeared to influence the work reported in this paper.

Acknowledgements

The authors would like to acknowledge Martin Quinn and Stuart Morse, for technical assistance in the fabrication and compressive testing of samples, and discussions with Prof Tom Mullin. FB was supported by EPSRC, UK through the grant EP/R045364/1. The research data supporting this publication are available in the supplementary materials.

Appendix A. Materials

Holey columns and sheets were machined (subtractive manufacturing) from commercial sheets of aluminium (alloy 5083, Smiths Metal Centres Ltd.), copper (alloy C101 and C110/OFHC, Smiths Metal Centres Ltd.), brass (alloy CZ121, Smiths Metal Centres Ltd.), nylon, polytetrafluoroethylene (PTFE), and polyether ether ketone (PEEK). Samples were also 3D printed (additive manufacturing) in polylactic acid (PLA) plastic (VeroBlue, Stratasys Ltd.) and a plastic composite reinforced with carbon fibre (Onyx, Markforged). Most 3D-plastic samples were produced on the same 3D printer (Objet30 Pro, Stratasys Ltd), although the sample made from a reinforced plastic composite was produced on a different printer (Onyx Pro, Markforged). Aluminium samples were annealed prior to testing. Control samples (cylinders of diameter 10 mm and height 15 mm) of each material were subject to compressive testing and the Young's modulus of the bulk, E_{bulk}, was calculated from the linear region of the resultant stress–strain data to be: 10.6 G Pa (aluminium), 2.0 G Pa (3D printed plastic – Vero Blue), 11.1 G Pa (brass), 11.0 G Pa (copper), 7.3 G Pa (OFHC copper), 0.6 G Pa (Nylon), 0.5 G Pa (PTFE), 2.8 G Pa (PEEK). The only material not to be tested for its bulk properties was the 3D plastic composite (reinforced with carbon fibre); the manufacturers value was reported to be $E_{bulk} = 1.4$ G Pa.

Appendix B. Supplementary data

Supplementary material related to this article can be found online at https://doi.org/10.1016/j.eml.2020.100980.

References

[1] K.E. Evans, M.A. Nkansah, I.J. Hutchinson, S.C. Rogers, Molecular network design, Nature 353 (1991).
[2] R.H. Baughman, J.M. Shacklette, A.A. Zakhidov, S. Strafstrom, Negative Poisson's ratios as a common feature of cubic metals, Nature 392 (1998).
[3] R. Lakes, K.W. Wojciechowski, Negative compressibility, negative Poisson's ratio, and stability, Phys. Status Solidi 245:3 (2008).
[4] G.N. Greaves, A.L. Greer, R.S. Lakes, T. Rouxel, Poisson's ratio and modern materials, Nature Mater. 10 (2011).
[5] K.K. Saxena, R. Das, E.P. Calius, Three decades of auxetics research - materials with negative Poisson's ratio: A review, Adv. Eng. Mater. 18 (2016).
[6] A. Papadopoulou, J. Laucks, S. Tibbits, Auxetic materials in design and architecture, Nat. Rev. Mater. 2 (2017).
[7] R.S. Lakes, Negative-Poisson's-ratio materials: Auxetic solids, Annu. Rev. Mater. Res 47 (2017).
[8] X. Ren, R. Das, P. Tran, T.D. Ngo, Y.M. Xie, Auxetic metamaterials and structures: A review, Smart Mater. Struct. 27 (2018).
[9] M. Shaat, A. Wagih, Hinged-3D metamaterials with giant and strain-independent Poisson's ratios, Sci. Rep. 10 (2020).
[10] T. Mullin, S. Deschanel, K. Bertoldi, M.C. Boyce, Pattern transformation triggered by deformation, Phys. Rev. Lett. 99 (2007) 084301.
[11] K. Bertoldi, M.C. Boyce, S. Seschanel, S.M. Prange, T. Mullin, Mechanics of deformation-triggered pattern transformations and superelastic behavior in periodic elastomeric structures, J. Mech. Phys. Solids 56 (2008) 2642–2668.
[12] K. Bertoldi, P.M. Reis, S. Willshaw, T. Mullin, Negative Poisson's ratio behaviour induced by an elastic instability, Adv. Mater. 22 (2010) 361–366.
[13] T. Mullin, S. Willshaw, F. Box, Pattern switching in soft cellular solids under compression, Soft Matter 9 (2013) 4951.
[14] B. Florijn, C. Coulais, M. van Hecke, Programmable mechanical metamaterials, Phys. Rev. Lett. 113 (2014) 175503.
[15] B. Florijn, C. Coulais, M. van Hecke, Programmable mechanical metamaterials: The role of geometry, Soft Matter 12 (2016) 8736–8743.
[16] K. Bertoldi, Harnessing instabilities to design tunable architectured cellular materials, Ann. Rev. Mater. Res. 47 (2017) 51–61.
[17] K. Bertoldi, V. Vitelli, J. Christensen, M. van Hecke, Flexible mechanical metamaterials, Nat. Rev. Mater. 2 (2017) 17066.
[18] H.M.A. Kolken, A.A. Zadpoor, Auxetic mechanical metamaterials, RSC Adv. 7 (2017).
[19] Y. Zhang, E.A. Matsumoto, A. Peter, P.-C. Lin, R.D. Kamien, S. Yang, One-step nanoscale assembly of complex structures via harnessing of an elastic instability, Nano Lett. 8(4) (2008).
[20] J.-H. Jang, C.Y. Koh, K. Bertoldi, M.C. Boyce, E.L. Thomas, Combining pattern instability and shape-memory hysteresis for phononic switching, Nano Lett. 9(5) (2009).
[21] X.L. Zhu, Y. Zhang, D. Chandra, S.C. Cheng, J.M. Kikkawa, S. Yang, Two-dimensional photonic crystals with anisotropic unit cells imprinted from poly (dimethylsiloxane) membranes under elastic deformation, Appl. Phys. Lett. 93 (2008) 161911.
[22] D. Krishnan, H. Johnson, Optical properties of two dimensional polymer photonic crystals after deformation induced pattern transformations, J. Mech. Phys. Solids 57 (2009) 1500–1513.
[23] S. Shan, S.H. Kang, P. Wang, C. Qu, S. Shian, E.R. Chen, K. Bertoldi, Harnessing multiple folding mechanisms in soft periodic structures for tunable control of elastic waves, Adv. Funct. Mater. 24 (2014) 4935–4942.
[24] J. Li, J. Shim, J. Deng, J.T.B. Overvelde, X. Zhu, K. Bertoldi, S. Yang, Switching periodic membranes via pattern transformation and shape memory effect, Soft Matter 8 (2012) 10322–10328.
[25] C.T. Nguyen, D.T. Ho, S.T. Choi, D.-M. Chun, S.Y. Kim, Pattern transformation induced by elastic instability of metallic porous structures, Comput. Mater. Sci. 157 (2019).
[26] J.W. Hutchinson, Plastic buckling, Adv. Appl. Mech. 14 (1974) 67–144.
[27] D.T. Ho, S.-D. Park, S.-Y. Kwon, K. Park, S.Y. Kim, Negative Poisson's ratios in metal nanoplates, Nat. Comm. 5 (2014).
[28] A. Ghaedizadeh, J. Shen, X. Ren, Y.M. Xie, Tuning the performance of metallic auxetic metamaterials by using buckling and plasticity, Materials 9 (2016).
[29] M. Taylor, L. Francesconi, M. Gerendás, A. Shanian, C. Carson, K. Bertoldi, Low porosity metallic periodic structures with negative Poisson's ratio, Adv. Mater. 26 (2014).
[30] D. Rayneau-Kirkhope, C. Zhang, L. Theran, M. Dias, Analytic analysis of auxetic metamaterials through analogy with rigid link systems, Proc. Roy. Soc. A 474 (2018).
[31] F. Box, R. Bowman, T. Mullin, Dynamic compression of elastic and plastic cellular solids, Appl. Phys. Lett. 103 (2013) 151909.
[32] D. Pihler-Puzović, A.L. Hazel, T. Mullin, The buckling of a holey column, Soft Matter 12 (2016) 7112–7118.
[33] C.G.J. Johnson, U. Jain, A.L. Hazel, D. Pihler-Puzović, T. Mullin, On the buckling of an elastic holey column, Proc. R. Soc. Lond. Ser. A Math. Phys. Eng. Sci. 473 (2017).
[34] C. Coulais, J.T.B. Overvelde, L.A. Lubbers, K. Bertoldi, M. van Hecke, Discontinuous buckling of wide beams and metabeams, Phys. Rev. Lett. 115 (2015) 044301.
[35] D. Correa, C. Seepersad, M. Haberman, Mechanical design of negative stiffness honeycomb materials, Integr. Mater. Manuf. Innov. 4 (2015).
[36] D. Debeau, C. Seepersad, M. Haberman, Impact behavior of negative stiffness honeycomb materials, J. Mater. Res. 33 (2018).
[37] E. Medina, P.E. Farrell, K. Bertoldi, C.H. Rycroft, Navigating the landscape of nonlinear mechanical metamaterials for advanced programmability, Phys. Rev. B 101 (2020).
[38] R. Maaß, P. Derlet, Micro-plasticity and recent insights from intermittent and small-scale plasticity, Acta Mater. 143 (2017).
[39] X. Zheng, W. Smith, J. Jackson, B. Moran, H. Cui, D. Chen, J. Ye, N. Fang, N. Rodriguez, T. Weisgraber, C.M. Spadaccini, Multiscale metallic metamaterials, Nature Mater. 15 (2016) 1100–1106.
[40] M. Li, J. Zuo, D. Hu, J. Shao, D. Liu, Experimental and numerical investigation of microstructure effect on the mechanical behavior and failure process of brittle rocks, Comput. Geotech. 125 (2020).
[41] C.R. Calladine, R.W. English, Strain-rate and inertia effects in the collapse of two types of energy-absorbing structure, Int. J. Mech. Sci. 26 (1984) 689–701.
[42] P. Qiao, M. Yang, F. Bobaru, Impact mechanics and high-energy absorbing materials: Review, J. Aerosp. Eng. 21 (2008).
[43] J. Brennan-Craddock, D. Brackett, R. Wildman, R. Hague, The design of impact absorbing structures for additive manufacture, J. Phys. Conf. Ser. 382 (2012) 012042.
[44] T. Wierzbicki, W. Abramowicz, On the crushing mechanics of thin-walled structures, J. Appl. Mech. 50 (1983).
[45] E. Wu, W. Jiang, Axial crush of metallic honeycombs, Int. J. Impact Eng. 19 (1997).
[46] S. Papka, S. Kyriakides, Biaxial crushing of honeycombs – Part 1: Experiments, Int. J. Solids Struct. 36 (1999).
[47] A.M. Hayes, A. Wang, B.M. Dempsey, D.L. McDowell, Mechanics of linear cellular alloys, Mech. Mater. 36 (2004).